



HAL
open science

Influence of silane interfacial chemistry on the curing process of anionic Polyamide 6 in glass reinforced composites

Achraf Belkhiri, Nick Virgilio, Enric Santanach-Carreras, Jérôme Esvan, Valérie Nassiet, Hélène Weleman, Olivier de Almeida, France Chabert

► **To cite this version:**

Achraf Belkhiri, Nick Virgilio, Enric Santanach-Carreras, Jérôme Esvan, Valérie Nassiet, et al.. Influence of silane interfacial chemistry on the curing process of anionic Polyamide 6 in glass reinforced composites. *Colloids and Surfaces A: Physicochemical and Engineering Aspects*, 2023, 676 (Part B), pp.132183. 10.1016/j.colsurfa.2023.132183 . hal-04200372

HAL Id: hal-04200372

<https://imt-mines-albi.hal.science/hal-04200372>

Submitted on 21 Sep 2023

HAL is a multi-disciplinary open access archive for the deposit and dissemination of scientific research documents, whether they are published or not. The documents may come from teaching and research institutions in France or abroad, or from public or private research centers.

L'archive ouverte pluridisciplinaire **HAL**, est destinée au dépôt et à la diffusion de documents scientifiques de niveau recherche, publiés ou non, émanant des établissements d'enseignement et de recherche français ou étrangers, des laboratoires publics ou privés.

Influence of silane interfacial chemistry on the curing process of anionic Polyamide 6 in glass reinforced composites

Achraf Belkhiri^{a,b}, Nick Virgilio^c, Enric Santanach Carreras^d, Jérôme Esvan^e, Valérie Nassiet^a, Hélène Weleman^a, Olivier De Almeida^{b,*} and France Chabert^a

^aLaboratoire Génie de Production (LGP), Université de Toulouse, INP-ENIT, Tarbes, France

^bInstitut Clément Ader, Université de Toulouse, CNRS UMR 5312, IMT Mines Albi, UPS, INSA, ISAE-SUPAERO, Albi, France

^cCREPEC, Department of Chemical Engineering, Polytechnique Montréal, Montréal, Canada

^dTotalEnergies SE, Pôle d'Etudes et de Recherche de Lacq, Lacq, France

^eCIRIMAT, Université de Toulouse, CNRS, INP-ENSIACET, Toulouse, France

ARTICLE INFO

Keywords:

Anionic ring opening polymerisation of PA6
Glass reinforcement
Silane sizing
polymerization kinetics.

ABSTRACT

The manufacturing of composites based on reactive thermoplastic polyamide 6 (PA6), reinforced with glass particles or fibers for structural applications, is quite sensitive to the state of the interface. Surface hydroxyls present at the glass surface can completely inhibit both the PA6 polymerization and crystallization processes. Care must then be exerted when tuning the interfacial chemistry in this system. This work demonstrates how an adequate choice of silane coupling agent, combined with a precise surface grafting methodology and tight control of hydroxyl groups density on glass particulates, yields kinetics and degrees of polymerization and crystallization comparable to the pure PA6 resin. Various silanes were grafted onto the microparticles and their surfaces were characterized by Fourier transform infrared spectroscopy, X-ray photoelectron spectroscopy, thermogravimetric analysis, confocal laser scanning microscopy and contact angle measurements. The activator was also grafted onto the glass surface to initiate polymerization directly from the surface. The results showed that all treated glass particles surfaces allowed obtaining a high degree of conversion but with varying polymerization and crystallization kinetics. The results provide fundamental information on the role of the surface chemistry of glass reinforcements on the polymerization and crystallization of PA6, which are essential for the proper control of composite manufacturing.

1. Introduction

With mechanical and chemical properties matching the requirements for structural applications, fiber reinforced thermoplastic composites are considered as a promising alternative to thermoset composites, since they can be welded, reshaped and recycled by using mechanical, thermal or chemical processes [1, 2, 3, 4, 5, 6, 7, 8]. Moreover, their storage at room temperature and their whole industrial supply chain is simplified compared to their thermoset counterparts.

However, manufacturing thermoplastic composite parts still remains a challenging issue due to the high melt viscosity of their matrices. Conventional liquid composite molding used for thermosets such as infusion or resin transfer molding (RTM) and their derivatives cannot be used directly in this case. Instead, fiber impregnation must be achieved throughout the whole fiber bed thickness using high pressure manufacturing processes [9]. In such context, low-viscosity reactive thermoplastic resins appear as a relevant option, as they are compatible with traditional liquid

*Corresponding author

✉ achraf.belkhiri@gmail.com (A. Belkhiri); nick.virgilio@polymtl.ca (N. Virgilio); enric.santanach-carreras@totalenergies.com (E. Santanach Carreras); jerome.esvan@toulouse-inp.fr (J. Esvan); valerie.nassiet@enit.fr (V. Nassiet); helene.weleman@enit.fr (H. Weleman); olivier.dealmeida@mines-albi.fr (O. De Almeida); france.chabert@enit.fr (F. Chabert)

manufacturing processes. They allow an in situ polymerization after impregnation of the reinforcements by the liquid resin.

Only a few polymers are suitable for this type of polymerization, and polyamide 6 (PA6) obtained by anionic ring-opening polymerization (AROP) exhibits the lowest viscosity prior to polymerization. It thus emerges as a relevant candidate for obtaining a homogeneous impregnation of textile preforms and achieving optimal overall behavior of the composites. In addition, PA6 polymerization is fast with a high degree of conversion and few parasitic reactions, which leads to good mechanical properties within a relatively short cycle time of synthesis [10, 11, 12].

PA6 synthesis by AROP is a well-known polymerization reaction, extensively studied by Malkin et al. in the 1980s [13, 14, 15, 16]. This reaction consists in using ϵ -caprolactam (ϵ -CL) as monomer, in combination with an activator and a catalyst [13, 17, 18]. The control of this reaction is complex due to the simultaneous polymerization and crystallization processes [13, 14, 15, 16, 19], but the recent development of reactive processing for textile fiber-reinforced thermoplastic composites has resulted in a renew of interest for this AROP process. In the early 2000s, Van Rijswijk et al. [20] investigated the reactive infusion of glass fibers/PA6 composites (GF/PA6). These authors have studied the effect of temperature, of the catalyst and activator chemistries and of their concentration on the PA6 synthesis kinetics. They have identified suitable conditions for obtaining a high degree of polymerization, but also underlined the importance of the interaction with the reinforcement as a particular point of attention.

Like all composites, the resulting mechanical properties not only depend on the choices of matrix and reinforcing particulates, but also strongly on the state and chemistry of the interface, e.g. the adhesion between the matrix and reinforcing particulates or fibers. The fiber-matrix interfacial interactions are therefore of prime importance for obtaining composite materials with optimal performances. But this point is even more critical when the matrix polymerization takes place in contact with the reinforcements of the composite. This is the case of all thermoset matrix composites and all composite materials involving a reactive thermoplastic matrix. Indeed, the surface of the fibers can interfere with the synthesis reaction, and in the particular case of anionic PA6 in contact with glass fibers, the hydroxyl groups on the glass surface deactivate the catalyst because of the labile protons. This leads to a slow-down or complete inhibition of the polymerization reaction, and ultimately to a significant reduction in the degree of conversion [12].

Since the combination of PA6 with untreated glass fibers is not suitable for anionic ring-opening polymerization [12], the use of a silane coupling agent is a worthy option to adapt glass fibers to reactive PA6. Moreover, the silane agent provides improved adhesion and stress-transfer at the fiber-matrix interface due to the formation of hydrogen bonds between the PA6 carbonyls and the primary amines of the silane [21, 22, 23]. Nevertheless, only a very few works have addressed the role of interfacial interactions between the grafted silane and a PA6 matrix during the anionic polymerization reaction, most likely because of the difficulty to properly tune and control the surface chemistry of glass fibers. The most significant study is certainly the work of Van Rijswijk et al. [23] who evaluated the mechanical

properties of AROP-based PA6 composites reinforced with silanized glass fibers. They emphasized the role of the silane coupling agent on the interfacial interaction between the matrix and fibers and the resulting consequences on the mechanical behavior.

Yet, this study only focuses on one type of aminosilane, and does not provide a detailed characterization of the reinforcements surface nor investigate the influence of the silane grafting on the polymerization process kinetics itself. It is therefore important to deepen and broaden the analysis of the surface chemistry of glass reinforcements in order to better control the polymerization and crystallization processes involved in reactive thermoplastics synthesis, and thus to improve the composites overall properties. This question is all the more important for in-situ polymerization of PA6 where the role of interfacial interactions is amplified, impacting both the fiber-matrix adhesion and the matrix synthesis process. This work then aims at understanding the impact of silane surface chemistry on the manufacturing of PA6/glass particulates composites, by preparing well controlled silanized glass surfaces and comparing the influence of different silane coupling agents on PA6 synthesis.

Grafting of a silane coupling agent can be achieved by substituting a fraction of the hydroxyl groups on the glass surface. However, the grafting of a silane agent onto a glass surface from an aqueous solution is a dynamic process, involving a competition between the silane condensation reaction at the surface, which consumes -OH groups, and the rehydroxylation process of siloxane groups, which increases the surface concentration of the hydroxyls. Therefore, in the case of anionic PA6, the silane grafting process must be particularly controlled, as too high a remaining -OH surface density can prevent the polymerization reaction to proceed after particles impregnation. This particular issue of the influence of the concentration of hydroxyl groups has been extensively studied by the authors in a previous work [24]. The result of this study led to the definition of an optimized grafting protocol that ensures efficient anionic ring-opening polymerization of ϵ -caprolactam, with a high degree of monomer conversion and silane grafting [24]. This optimized silane grafting protocol is used in this study for the grafting of various silane coupling agents.

The original contribution of this work lies in the broad study of several silane chemistries, leading to distinct interfacial interactions with the PA6 matrix, and allowing the investigation of their impacts on the polymerization and crystallization: (i) First, a hydrophobic silane minimizing the interfacial interactions; (ii) Second, two aminosilanes forming hydrogen bonds with the PA6 matrix; (iii) Third, a grafted silane also bearing the covalently linked activator that initiates the polymerization from the glass surface, and generates covalent bonds at the interface.

A systematic and rigorous characterization of the silanized glass surface is performed by means of several complementary techniques in order to deeply understand the surface chemical modifications involved (Fourier transform infrared spectroscopy (FTIR), X-ray photoelectron spectroscopy (XPS), thermogravimetric analysis (TGA), confocal laser scanning microscopy (CLSM) and contact angle measurements). Finally, the impact of the nature of

the silane on the polymerization and crystallization kinetics is evaluated via DSC measurements, making it possible to characterize the physical and chemical properties of the synthesized PA6.

2. Experimental

2.1. Materials and their preparation

2.1.1. AROP reactants selection and preparation

Anionic ring opening polymerization of PA6 is performed using ϵ -caprolactam AP-NYLON ®(ϵ -CL) as monomers, caprolactam magnesium bromide (MgBrCL - Nyrin ®C1, at 1.4 mol.kg⁻¹ in caprolactam) as the catalyst, and bifunctional hexamethylene-1,6-dicarbamoylcaprolactam (HDCL- Brggolen ®C20P at 2.0 mol.kg⁻¹ in caprolactam) as the activator. All products were kindly supplied by Brüggemann Chemical, Germany. Since storage and processing have to be conducted in a moisture free environment due to the sensitivity of the reaction to water, the products were dried overnight at 30°C under vacuum before each synthesis. Then, all handling was carried out in an inert atmosphere in a glove box. The reactants being solid at room temperature, the mixture was obtained by first melting the monomer in a beaker using a heating magnetic stirrer (T_m (ϵ -CL) = 69°C), and then by sequentially incorporating the catalyst and the activator under moderate stirring. The MgBrCL/HDCL ratio was 0.79/1.10 mol% based on the CL content.

2.1.2. Glass particles

In order to avoid the combined influences of fiber length and orientation, glass microparticles of a size representative of glass fiber diameters were used. Glass microparticles were purchased from SOVITEC (France) with an average diameter of 4 μ m. A SEM micrograph of the raw glass particles is presented in Figure S1 in the Supporting Information file. The particle size was chosen in order to have: (1) a specific surface representative of glass fiber reinforced composites, i.e. equivalent to a fiber volume content of 60% with 5 μ m diameter glass fibers, and (2) to obtain a glass volume fraction not exceeding 30% in order to facilitate the mixing process during the mixture preparation.

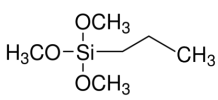
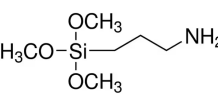
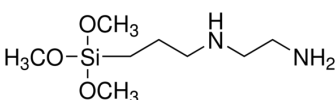
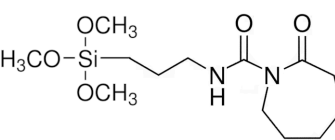
Before silanization, the particles were calcinated in an oven at 450°C for 10 h according to the treatment protocol defined by the authors in a previous work [24]. This condition makes it possible to limit the amount of residual surface hydroxyls after silane grafting that slow down or even deactivate the polymerization reaction.

2.1.3. Silanes selection and synthesis

The chemical structures of four types of silanes, and the expected interactions with the anionic PA6 matrix, are presented in Table 1. The first three silanes were purchased from Fisher Scientific and used as received. Trimethoxy(propyl)-silane (TMPS, 98%) was selected to generate a hydrophobic surface with minimum expected interactions with the PA6 matrix. The other two belong to the aminosilanes family commonly used in the sizing

Table 1

Name and structure of the considered silanes and related interfacial interactions expected with the anionic PA6 matrix

| Name | Chemical structure | Interaction with anionic PA6 |
|--|---|------------------------------|
| Trimethoxy(propyl)-silane (TMPS, 98%) |  | Low interactions |
| (3-Aminopropyl)trimethoxysilane (APTMS, 97%) |  | Weak hydrogen bonds |
| 3-(2-Aminoethylamino)propyltrimethoxysilane (AEAPTMS, 96%) |  | Weak hydrogen bonds |
| 2-oxo-azepane-1-carboxamide-N-[3-(propyl)]-trimethoxysilane (ACTISILANE) |  | Strong covalent bonds |

formulations of the major glass fiber manufacturers [25]. The two aminosilanes terminated with primary amines were used to create hydrogen bonds between the glass particles and the PA6 matrix. (3-Aminopropyl)trimethoxysilane (APTMS, 97%) was chosen as it is currently used with anionic glass reinforced PA6 and is therefore an adequate system for comparison purposes [12, 21, 22, 23]. In contrast, 3-(2-Aminoethylamino)propyltrimethoxysilane (AEAPTMS, 96%) could be a better candidate for surface modification, since it can create stable silanol bonds due to the secondary amine groups. In addition, this silane leads to reproducible silane layers [26].

The fourth silane (named ACTISILANE) is terminated with the N-acetylcaprolactam function of the activator. Although it is specific, this function was selected as it remains compatible with other lactam polymerization reactions, like the polymerization of lauryl-lactam for the synthesis of Polyamide 12, and allows the formation of strong covalent bonds between the glass particle surface and the PA6 matrix. A similar approach is described in a patent by Johns Manville [27], without detailing the resulting molecular structure, or the silane synthesis protocol. For this reason, the following protocol was set specifically for our study.

The ACTISILANE was synthesized by adding 3-isocyanatopropyltrimethoxysilane (IPTS, 95%) and the monomer ϵ -CL in a hydrophobic beaker under inert atmosphere in a glove box. The mixture was then heated to 70°C and left to react for 72 h. The isocyanate function present in IPTS has a high reactivity due to its strong polarization. Indeed,

the carbon with a partially positive charge is located between the more electronegative nitrogen and oxygen atoms, which results in a high electrophilicity. This electrophilicity makes the isocyanate very reactive towards nucleophiles, especially amines. Initially, the electrophilic carbon of the isocyanate function is attacked by the free electron pair of the nitrogen present in the amide function of the caprolactam. This results in the formation of urea and carboxamide functions. In a second step, a proton exchange leads to the formation of the N-acetylcaprolactam function. The mechanism of the reaction is shown in Figure 1.

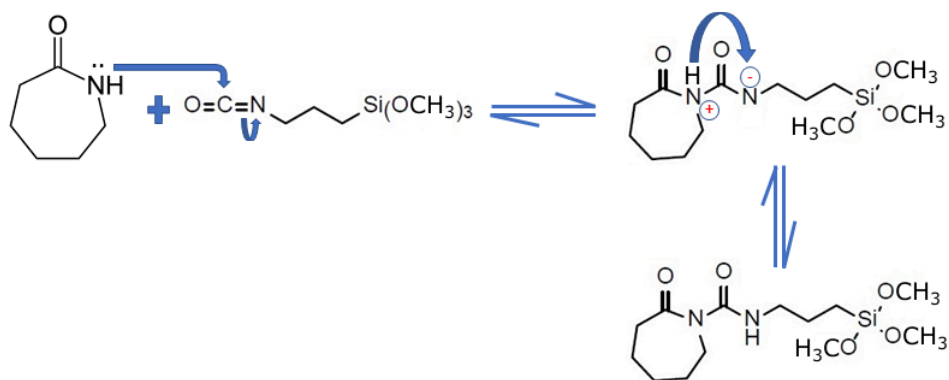


Figure 1: Reaction mechanism for the synthesis of the ACTISILANE coupling agent.

The synthesized ACTISILANE was characterized with a Fourier transform infrared spectrometer Perkin Elmer Spectrum One in Attenuated Total Reflectance (ATR) mode to verify the efficiency of the reaction and to ensure the formation of the N-acetylcaprolactam function. A Diamant/ZnSe crystal was used and the spectra were measured in a wavelength range between 650 and 4000 cm^{-1} with a resolution of 1 cm^{-1} . The characterization results are presented in the supporting information file (Section 2).

2.1.4. Silane grafting

After calcination, the glass particles were simultaneously rehydroxylated and silanized for 2 h. This protocol provides significant silane grafting onto the glass surface, while limiting the presence of residual hydroxyl groups [24]. The silanes were added to an aqueous solution at 5% (v/v). The pH was then adjusted to 4-5 since acidic conditions promote the formation of silanols while slowing down self-condensation between the resulting hydrolyzed silanol groups [28]. This was achieved using acetic acid, in the same way as Brochier et al. [28]. The mixture was stirred for about 45 min. After silane hydrolysis, the glass particles were added to the solution and stirred for 1 h. The mixture was then kept at 100°C for 1 h to condense the silanol groups on the surface and to remove traces of methanol from the hydrolysis of the methoxysilanes. Finally, the particles were rinsed twice with ethanol and twice with water to remove the unreacted silanes, before drying for 2 h at 115°C. The same grafting protocol was used for all of the silanes, except

for the case of the ACTISILANE, for which water was replaced by ethanol since the synthesized silane was not soluble in water.

2.2. Particle surface characterization

The silanized particles were characterized by Fourier transform infrared spectroscopy (FTIR), X-ray photoelectron spectroscopy (XPS), confocal laser scanning microscopy (CLSM), thermogravimetric analysis (TGA), and contact angles. The results were compared to calcinated particles (untreated particles), as a reference, to evaluate the extent of surface modification.

2.2.1. FTIR spectroscopic measurements

FTIR analyses in transmission mode were performed on a Bruker Vertex 70 spectrometer. Untreated and surface modified glass particles were mixed with high purity infrared grade KBr powder at 1.5-2 wt%, and pressed into pellets. The spectra were measured between 400 and 4000 cm^{-1} at a 2 cm^{-1} resolution. A background was obtained with a pure KBr pellet before measuring the spectra of each glass particle sample.

2.2.2. X-ray photoelectron spectroscopy (XPS)

The photoelectron emission spectra were recorded using a monochromatic Al K-alpha ($h\nu = 1486.6 \text{ eV}$) source on a ThermoScientific K-Alpha system. The X-ray spot size was about 400 μm . The pass energy was fixed at 30 eV with a step of 0.1 eV for core levels and 160 eV for surveys (step of 1eV). The spectrometer energy calibration was done using the Au 4f7/2 ($83.9 \pm 0.1 \text{ eV}$) and Cu 2p3/2 ($932.8 \pm 0.1 \text{ eV}$) photoelectron lines. XPS spectra were recorded in direct mode N (Ec) and the background signal was removed using the Shirley method. A flood gun was used to neutralize charge effects on the top surface. High resolution spectra are deconvoluted with the Avantage software from ThermoScientific to separate the contribution of each chemical element and on its chemical environment.

2.2.3. Confocal laser scanning microscopy (CLSM)

To visualize the efficiency of the surface treatments, the glass particles were treated with fluorescein 5-isothiocyanate (FITC) and observed by confocal microscopy. 1 mg of FITC (Fisher Scientific) was dissolved in 10 ml of absolute ethanol. Then, 10 mg of silanized glass particles were added to the solution. The mixture was stirred for 16 h in the dark at room temperature. The particles were next rinsed twice with ethanol and twice with water to remove the unreacted FITC. The FITC-labeled glass particles were finally dispersed in DMSO during measurements in order to reduce the refractive-index mismatch between the suspending media, the particles and the microscope cover slip. All images were taken using a laser scanning Leica SP8 confocal microscope and with the same lighting conditions to get semi-quantitative comparison values. A PMT detector collected light emitted in the range of 501-681 nm. Excitation of the fluorophore was ensured with a laser at $\lambda_{\text{ex}} = 488 \text{ nm}$, and the laser was set to 0.2% of its

full-power. An oil-immersion 40X objective with a numerical aperture of 1.3 was used. The images were acquired with the microscope set to the resonant mode and by doing 8-lines averages to improve the signal-to-noise ratio. The pinhole was set at 1 Airy Unit ($61 \mu\text{m}$), which results in an optical section thickness of $0.985 \mu\text{m}$. The images resolution was 1024×1024 pixels, representing an area of $42.7 \times 42.7 \mu\text{m}^2$. The zoom factor was 6.81.

2.2.4. Thermogravimetric Analysis (TGA)

The weight loss of the glass particles following the different thermal and chemical treatments was monitored with a Mettler Toledo TGA1 STARe System. The glass particles were heated from 25°C to 450°C at $10^\circ\text{C}/\text{min}$ under air flow, then held at this temperature for 15 h until the mass stabilized. This temperature was chosen in agreement with the temperature of the first calcination step.

2.2.5. Contact angles

The contact angles of pristine and surface-modified particles were measured at 25°C with a DIGIDROP goniometer from GBX equipped with a white light source and a KRÜSS camera. Flat surfaces were prepared by compressing particles into pellets. $10.5 \mu\text{l}$ drops of deionized water were carefully deposited on the sample surface. This volume was chosen to ensure that the drop would detach and fall on the surface by gravity. Images were acquired automatically at 24 frames per second. The first image after the water drop falls on the glass particles surface was selected as a reference for measuring the contact angle values. The dynamic contact angle was also analyzed by measuring the contact angle value over time on successive images. The contact angle was recorded every 0.1 s.

2.3. Synthesis and characterization of PA6 and of PA6/particles composites by differential scanning calorimetry (DSC)

The syntheses of PA6/particles composites were monitored with a power-compensated Perkin-Elmer 8500 Differential Scanning Calorimeter (DSC) under nitrogen. The polymerization and crystallization kinetics were followed under isothermal conditions.

In the case of PA6/glass particle composites, a small quantity of glass particles was added first into the pan, for either untreated or surface modified particles. Then, the reactive monomer mixture (monomer, catalyst and activator) was added, targeting a particle content of 30 % (v/v) and a total weight of 10-12 mg. As a reference, neat resin samples were prepared by adding 4-10 mg of the reactive mixture in hermetically sealed aluminum pans under an inert atmosphere to prevent monomer evaporation and moisture absorption.

The DSC samples were first heated from 25°C to 180°C at $300^\circ\text{C}\cdot\text{min}^{-1}$, and the temperature was then kept constant for 50 min. This thermal treatment makes it possible to decouple the polymerization and crystallization processes and, therefore, to identify their respective kinetics parameters [19]. Finally, the samples were cooled to 0°C at $-10^\circ\text{C}\cdot\text{min}^{-1}$.

After cooling, each sample was heated again from 0°C to 270°C at 10°C.min⁻¹ to obtain the melting temperature (T_m) and melting enthalpy (ΔH_m) of the crystalline phase.

3. RESULTS AND DISCUSSION

3.1. Particle surface characterization

3.1.1. FTIR

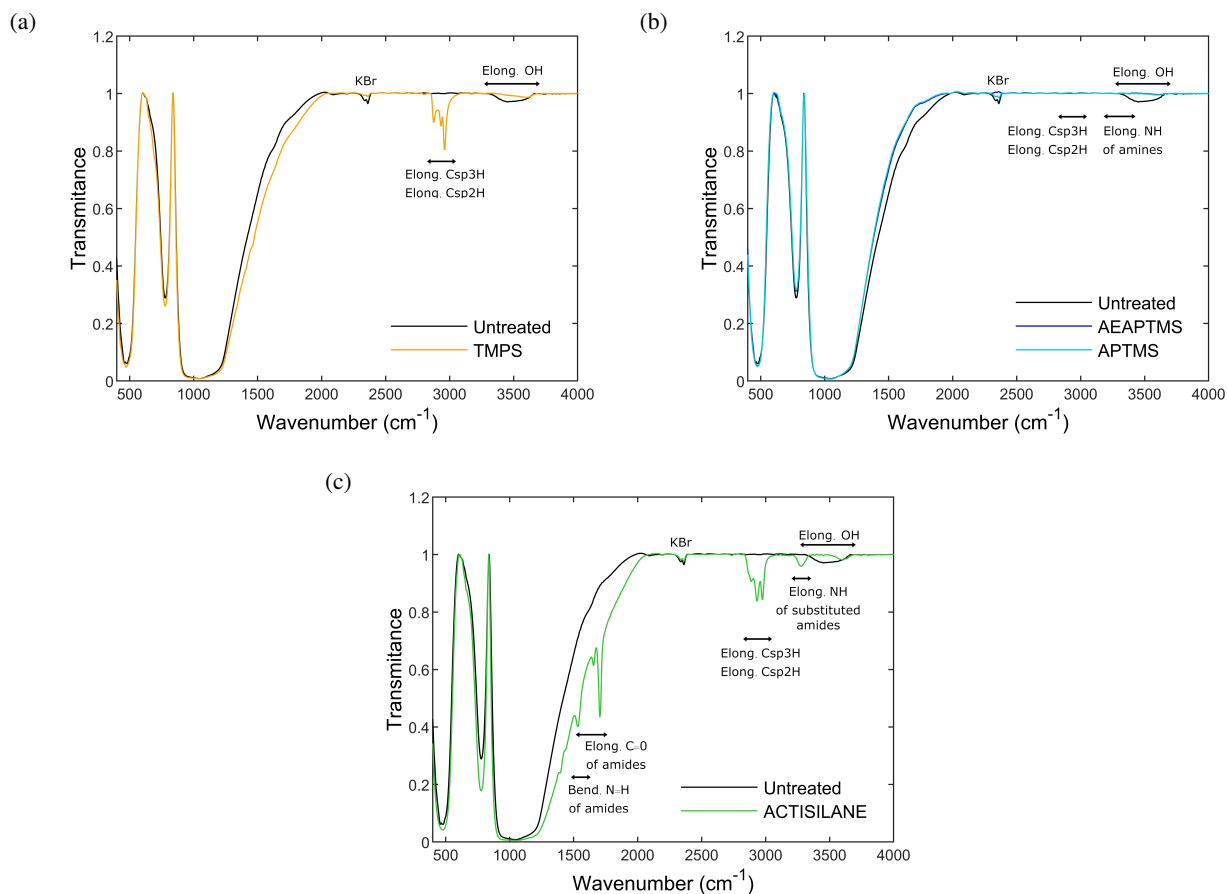


Figure 2: FTIR spectra of untreated particles compared to the spectra of particles treated with (a) TMPS, (b) APTMS and AEPTMS, and (c) ACTISILANE

The spectra of untreated and TMPS treated particles are compared in Figure 2a. The appearance of a number of bands between 2850 and 2970 cm⁻¹ is typical of CH₂ and CH₃ bonds, and confirms the presence of grafted silanes on the surface of the treated particles. Moreover, the band at 3500 cm⁻¹ related to hydroxyl groups that can be observed in the spectra of the untreated particles almost disappears in the spectra of the treated ones. This confirms the consumption of -OH groups during the condensation reaction with silanes, although the acidic conditions of silanization can induce some hydroxylation of the glass surface [24].

Figure 2b shows the spectra of the particles treated with APTMS and AEAPTMS, compared to the spectra of the untreated particles. As in the previous case, the reduction of the band at 3500 cm^{-1} related to the -OH groups indicates the reaction of these groups with the silanes. However, the spectra do not show the presence of the amine group bands on the surface of the particles. Indeed the N-H function stretching vibration should appear between 3250 and 3450 cm^{-1} , and a band between 1530 and 1650 cm^{-1} related to the bending vibration. These bands are not obvious in the signals. Thus, other techniques of surface characterization are necessary in order to further analyze the surface and confirm the presence and the retention of the amine groups on the surface after grafting.

Figure 2c shows the spectra of particles treated with the ACTISILANE, the case of untreated particles being given as a reference. The ACTISILANE functions on the surface of the treated particles are obvious: first, the bands between 2850 and 2970 cm^{-1} are associated to the presence of CH_2 groups. Then, the bands at 3280 and 1536 cm^{-1} correspond to the N-H bond of the urea function initially visible in the spectra of the synthesized ACTISILANE (see Section 2 in the Supporting Information file) which reappears in the spectra of the treated particles, confirming its successful grafting and the retention of the chemical functions. The same result is observed for the bands at 1657 cm^{-1} and 1702 cm^{-1} , related to carbonyl groups. On the other hand, the intensity of the band at 3500 cm^{-1} (hydroxyls) in the spectra of the untreated particles decreases for the spectra of the treated particles and even shifts to 3600 cm^{-1} . The wavenumber strongly depends on the interactions between the hydroxyl groups, and their environment. When hydroxyl groups are involved in hydrogen bonds, the associated wavenumber decreases [29]. In the case of untreated particles, the hydroxyls are sufficiently close to each other to create hydrogen bonds. When the hydroxyls are removed during the reaction with the silane, the -OH groups remaining at the surface become progressively isolated, which shifts the signal to higher wavenumbers.

3.1.2. XPS

XPS allows a finer analysis of the chemical composition of a surface, and allows to identify the elements by assuming an analysis depth less than 10 nm. This analysis is complementary to the FTIR investigation to check for the presence and the conservation of the grafted chemical functions, in particular the amine functions of the particles treated with the aminosilanes - not detected on FTIR spectra - and the N-acetylcaprolactam function. Three samples were selected for the XPS analysis. First, the untreated particles were used as a reference. Second, the APTMS treated particles were analyzed since the alkyl chain of this silane is simpler to interpret than AEAPTMS. In addition, APTMS is more commonly used, which allows a comparison with the literature. Finally, the particles treated with the ACTISILANE were considered since this silane exhibits a rather complex termination and requires an extensive analysis due to its novelty.

Table 2

Identification and quantification of elements from XPS analysis for the untreated particles, and particles treated with APTMS and ACTISILANE

| Atoms | Binding Energy (BE) | Atomic (%) | | |
|----------|---------------------|------------|--------|------------|
| | | Untreated | APTMS | ACTISILANE |
| Si 2p | 103.1 | 16.0 | 16.7 | 12.3 |
| C 1s | 285.0 | 35.4 | 41.0 | 43.2 |
| O 1s | 532.0 | 38.6 | 34.0 | 32.5 |
| N 1s | 400.0 | - | 2.4 | 2.7 |
| Na 1s | 1701.4 | 6.1 | 3.7 | 6.5 |
| Ca 2p3/2 | 346.2 | 1.9 | 1.4 | 1.5 |
| Mg 1s | 1303.1 | Traces | Traces | Traces |

The ratios of elements on the surface of the particles are compared in Table 2. Silicon, calcium, oxygen, sodium and magnesium are specific to glass particles, while carbon, oxygen and nitrogen come from the silanes. A significant amount of carbon is also detected on the surface of the untreated particles, which can come from atmospheric pollution and the carbon tape used to support the particles. Since all the samples were prepared in such a way, comparing the evolution of the ratios after grafting is relevant.

The evolution of the C/Si and O/Si ratios are preferred in the literature to characterize coupling agents [30, 31]. The results in Table 3 show an increase of the C/Si ratio after the grafting of both silanes in agreement with the higher number of carbons in the grafted chains. The O/Si ratio varies as a function of the type of silane: it decreases in the case of APTMS because grafting reduces the amount of oxygen (only the oxygen of silanols after hydrolysis is still present). Thus, the amount of grafted oxygen is lower than the amount of grafted silicon. However, this ratio increases in the case of the ACTISILANE because oxygen atoms remain in its structure. The quantity of grafted oxygen is thus higher compared to the quantity of grafted silicon. Accordingly, the C/Si ratio increases more than the C/O ratio in the case of the ACTISILANE, which is the opposite trend to what is observed for APTMS. Nitrogen is not present on the surface of untreated particles, but it appears on the surface of silanized particles. This supports not only the presence of the silanes on the surface of the treated particles, but also the preservation of the amine functions after grafting. For both types of grafted surfaces, the N/Si ratio is lower than 1, which is consistent with the literature and is explained by the significant presence of Si on the glass particle surface [31].

However, since silicon, carbon and oxygen are present both in the silanes and at the surface of the untreated particles, the calculated ratio relative to silicon can be affected by the change in the silicon percentage according to the silane type. In order to overcome this limitation, it is interesting to focus on an element specific to the surface of glass particles and that is not present in the silane, i.e. calcium. Indeed, the use of various modifying oxides during the glass manufacturing is reflected as traces in its final composition. In particular, the use of calcium oxide to increase the chemical resistance, luster and decrease the solubility of glass leads to the appearance of calcium on its surface during XPS analysis. The

Table 3

Atomic concentrations relative to silicon and calcium, for untreated particles and particles treated with APTMS and ACTISILANE

| Atoms | /Si | | | /Ca | | |
|-------|-----------|-------|------------|-----------|-------|------------|
| | Untreated | APTMS | ACTISILANE | Untreated | APTMS | ACTISILANE |
| C | 2.2 | 2.4 | 3.5 | 18.4 | 29.3 | 30.4 |
| O | 2.4 | 2.0 | 2.6 | 20.1 | 24.3 | 22.9 |
| N | - | 0.1 | 0.2 | - | 1.7 | 1.9 |
| Si | - | - | - | 8.3 | 11.9 | 8.7 |
| C/O | 0.9 | 1.2 | 1.3 | 0.9 | 1.2 | 1.3 |

C/Ca, O/Ca and Si/Ca ratios are given in Table 3. Previous comparisons based on silicon are confirmed by respective ratios based on calcium, which supports the successful grafting of silanes on the surface of glass particles. The increase of the O/Ca ratio in the case of APTMS is noteworthy, contrary to the O/Si ratio. Indeed, the grafted silane contains silicon and oxygen atoms specific to the silanol function, but it does not contain calcium. Thus, silane grafting increases the O/Ca ratio whereas the O/Si ratio decreases since the added silicon after grafting is higher than oxygen.

3.1.3. Confocal fluorescence microscopy

In order to confirm the XPS results showing the presence of nitrogen, and to confirm the retention of the primary and secondary amine functions on the surface of the particles treated with APTMS and the ACTISILANE, confocal fluorescence microscopy was used. For that purpose, fluorescein 5-isothiocyanate (FITC) was grafted and used as a probe to identify the presence of amines. The isocyanate group reacts with primary and secondary amines to form stable urea functions.

The images obtained by confocal microscopy are shown in Figure 3. Figure 3a displays the untreated particles, as a reference, while Figure 3b shows the TMPS grafted particles. For these two cases, the low level of fluorescence can be attributed to the non-specific adsorption (physisorption) of FITC, as the $-N=C=S$ groups of FITC selectively react with $-NH_2$ and NH groups, while no reaction occurs with the other surface functions under the considered grafting conditions. In addition, the raw glass particles not treated with FITC do not exhibit any fluorescence under the same observation conditions (see Figure S4 in Supporting information). Next, the glass particles treated with the aminosilanes display higher fluorescence intensity compared to the untreated particles, involving the presence of amine functions (Figure 3c, 3d). Their respective fluorescence intensities are quantified in Figure 4.

The particles treated with AEAPTMS show a higher fluorescence level compared to those treated with APTMS. This is due to the presence of both primary and secondary amines on the AEAPTMS chains, while APTMS only contains primary amines. In addition, the silane multilayers formed by APTMS by vertical polymerization generate a higher steric hindrance than AEAPTMS which, in contrast, forms more homogeneous silane layers [32, 26]. This increases the number of accessible amine functions in the particles treated with AEAPTMS, thus increasing their

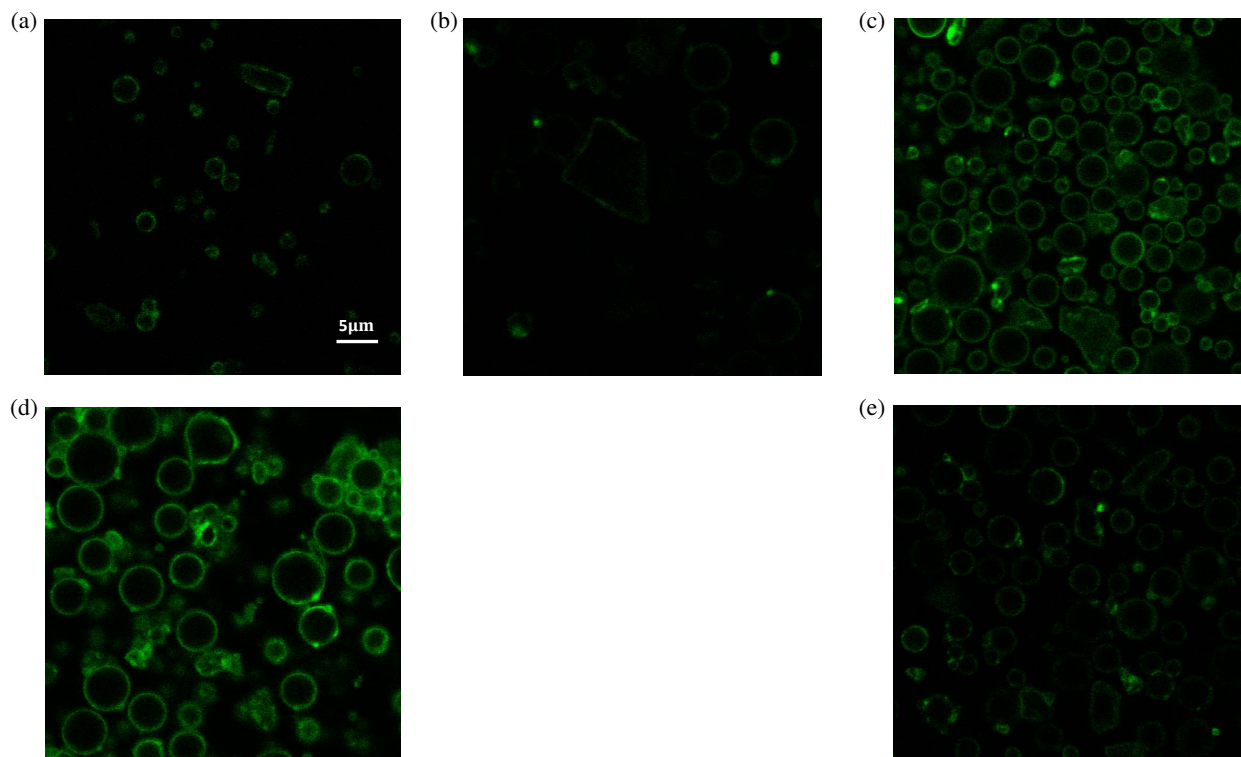


Figure 3: Confocal fluorescence microscopy images of (a) untreated particles, compared to particles treated with (b) TMPS, (c) APTMS, (d) AEAPTMS, and (e) the ACTISILANE.

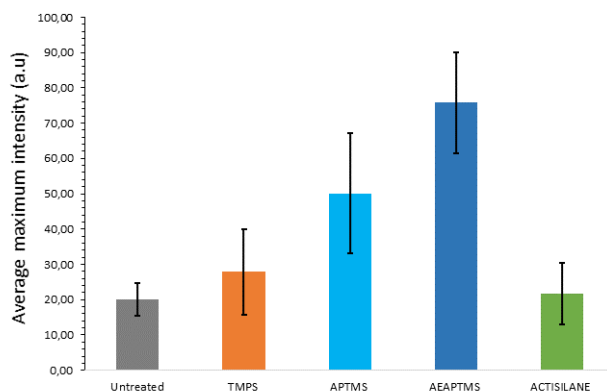


Figure 4: Average maximum fluorescence intensity of untreated particles, compared to particles treated with APTMS, AEAPTMS, and the ACTISILANE. At least 36 particles were considered for each type of surface treatment. The error bars correspond to the standard deviation.

reactivity with the FITC agent. Overall, these results confirm the retention of amine groups following the grafting of both APTMS and AEAPTMS silanes.

Finally, the very low fluorescence level observed for the ACTISILANE treated particles (Figure 3e) can also be explained to the physisorbed FITC on the surface, since the intensity is lower than TMPS treated particles and

Table 4

TGA mass loss of silanized particles compared to the mass loss of untreated particles. The mass loss related to silane and the silane surface density are noted Δm_{silane} and d_{silane} respectively

| Particle type | Total mass loss ($\pm 0.05\%$) | FTIR Transmittance at 3500 cm^{-1} (%) | Δm_{silane} (%) | d_{silane} (molecule.nm ⁻²) |
|---------------|-------------------------------------|--|----------------------------|--|
| Untreated | 0.14 | 93.12 | - | - |
| TMPS | 2.26 | 94.69 | 2.17 | 184 |
| APTMS | 1.33 | 95.51 | 1.27 | 89 |
| AEAPTMS | 0.71 | 95.51 | 0.65 | 30 |
| ACTISILANE | 2.02 | 94.11 | 1.91 | 51 |

close to the untreated particles case. Indeed, although the particles treated with ACTISILANE contain a secondary amine function as demonstrated by FTIR and XPS, this function does not react with the FITC agent. The grafted ACTISILANE and FITC are both relatively bulky molecules. Hence, the secondary amine functions present on the grafted ACTISILANE are inaccessible to the FITC molecules because of a steric effect, which prevents the reaction between FITC and the ACTISILANE secondary amines.

Confocal fluorescence microscopy therefore confirms the grafting efficiency and the presence of amine groups on the surface of the particles treated with the aminosilanes, in agreement with previous results given by FTIR and XPS.

3.1.4. TGA

Thermogravimetric analysis was used to quantify the surface density of the grafted silanes. In this way, the mass loss related to the residual hydroxyl groups was subtracted from the total mass loss of the silanized particles after calcination, following a procedure described in a previous work [24]. The results are displayed in Table 4.

The total mass loss for the untreated particles is 0.14%, corresponding to the loss of -OH groups. For the treated particles, the mass loss related to residual -OH groups can be calculated from the mass loss of whole hydroxyls groups and from of the residual hydroxyls surface density d_{OH} (OH.nm⁻²). The latter is given by Equation 1:

$$d_{OH} = -22.71T + 2208.38 \quad (1)$$

where T (%) is the transmittance band at 3500 cm^{-1} obtained by FTIR.

After subtracting the mass loss related to -OH groups, the results still show a considerable mass loss related to the silane groups, confirming again significant silane grafting on the surface. Equation 2 gives the grafted silane surface density d_{silane} (molecule.nm⁻²):

$$d_{silane} = \frac{\Delta m_{silane} * Na}{100 * M * S} \quad (2)$$

in which Δm_{silane} is the silane mass loss measured by TGA (%), N_A is Avogadro's constant, M is the silane molecular weight ($\text{g}\cdot\text{mol}^{-1}$), and S is the specific surface area of glass the particles obtained by BET ($\text{nm}^2\cdot\text{g}^{-1}$).

The results are displayed in Table 4, and are relatively high compared to literature values reported for alkoxy silane monolayers (between 2.1 and 4.2 molecules per nm^2) [33, 34, 35, 36]. Several authors have shown that such an overestimation may come from the specific surface measurement technique [29, 37, 38]. Indeed, the specific surface area used in the calculation is obtained by the BET technique. This method is based on the adsorption of nitrogen gas, but it was demonstrated that a large fraction of the microporosities on the surface are not accessible to nitrogen molecules at 77 K, and therefore are not considered in the measurement [29, 37, 39, 40, 41, 42]. SEM micrographs (see Figure S5, in Section 4 of the Supporting information file) show that the glass particles used in the present study form aggregates, which generates very fine microporosities not necessarily detectable by BET analysis. The specific surface area could therefore be underestimated, leading to overestimated surface density values. On the other hand, it is also possible to find high grafting densities due to the formation of silane multilayers [43, 44]. For example, De Palme et al. found a density of 29 molecules per nm^2 for a grafted aminosilane on ferrite nanoparticles by a TGA measurement [43].

The silane density on the surface of treated particles also depends on the silane nature, and especially its reactive functions. Indeed, the nature of the organofunctional groups on each silane has a role in the hydrolysis and condensation kinetics and, consequently, it influences the grafting kinetics [28, 45]. For example, Asenath et al. [32] showed that amine groups can catalyze, either inter- or intramolecularly, the reaction between silane molecules and surface silanol groups to form siloxane bonds. For this reason, aminoalkoxysilanes are more reactive in water than alkylalkoxysilanes. Therefore, grafted aminoalkoxysilanes can block neighboring surface hydroxyls via two-dimensional self-assemblies (horizontal polymerization) and local multilayers (vertical polymerization) for APTMS, and by the steric hindrances caused by the longer chain length for AEAPTMS. This explains the lower grafting density obtained for the aminosilanes compared to TMPS. The ACTISILANE is the largest molecule and also leads to important steric hindrances. Its grafting density stands in the same range as AEAPTMS, again quite far from TMPS.

It is quite difficult to obtain similar grafting densities with different silanes because each has its own grafting kinetics. The factors influencing this kinetics (silane concentration and/or silanization time) also influence the quantity of residual hydroxyl groups, which could negatively impact the polymerization kinetics. All this makes the control of the grafting density rather complex.

Table 5

Contact angles of untreated and treated particles according to the type of treatment and expected type of interactions with the PA6 matrix.

| Expected interaction with PA6 | Treatment type | Contact angle ($^{\circ}$) \pm 1 |
|-------------------------------|------------------------|--------------------------------------|
| - | Untreated (calcinated) | 0 |
| Low chemical interaction | TMPS | 103 |
| Weak bonds | APTMS | 35 |
| Weak bonds | AEAPTMS | 19 |
| Strong bonds | ACTISILANE | 28 |

3.1.5. Contact angles

Next, the surface polarity of the treated particles was analyzed in terms of wettability, via the measurement of contact angles using disks of compressed particles. This allows to monitor the evolution of the hydrophilic/hydrophobic character of the surface after the silanization treatment, since PA6 has a hydrophilic character.

Table 5 shows the contact angles of both untreated and silanized particles. The contact angle of the untreated particles is zero, and the water drops are absorbed immediately after touching the surface. The surface of the untreated particles is, as expected, quite hydrophilic due to the large number of -OH groups present on their surface. The contact angle is higher for the silanized particles, and it reaches 103° for the TMPS case. Such increase again confirms the presence of the grafted silane layer at the surface of the treated particles, and values obtained stand in agreement with the literature [31, 46, 47, 48].

The difference in contact angle values between the treatments is due to the nature and surface density of the grafted silanes. Indeed, the treatments for which hydrogen bonds with PA6 are expected contain hydrophilic functions, especially primary and secondary amines. These functions increase the hydrophilicity of the surface and decrease the contact angle to a value below 90°. On the other hand, TMPS possesses non-polar $-CH_3$ end groups and yields to a hydrophobic surface, which significantly increases the contact angle value. The different wettability behavior may also be explained by the silane surface density. Indeed, confocal microscopy suggests that AEAPTMS bears more accessible amine functions compared to APTMS, which could increase the hydrophilicity of AEAPTMS. Therefore, the contact angle results follow a trend similar to the grafting density values, as described in Table 4.

In order to confirm these trends, dynamic contact angles are plotted as a function of time, until the drop was totally absorbed (except in the case of the TMPS treatment where the drop remains on the surface). Theoretically, the adsorption rate decreases with a decrease in surface hydrophilicity, which corresponds to an increase in static contact angle [46]. As shown by Figure 5, the dynamic measurements are thus consistent with the static ones.

The evolution of the water drop contact angle is a way to predict the level and types of interactions between the particles and the hydrophilic PA6 matrix. The TMPS treatment is highly hydrophobic, which should minimize the

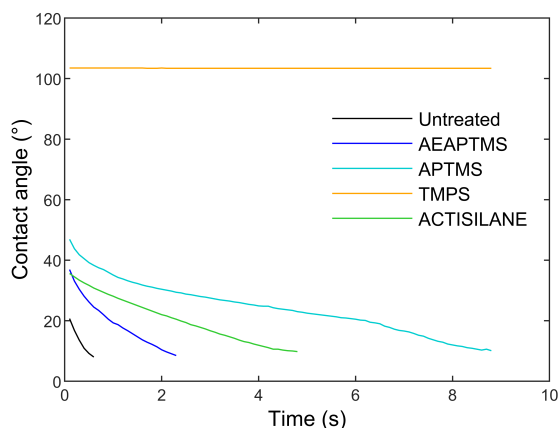


Figure 5: Evolution of the water drop contact angle as a function of time, for the different silane treatments.

PA6/particles interactions. In contrast, the particles treated with AEAPTMS, APTMS and the ACTISILANE should promote stronger interfacial interactions.

3.2. Influence of the surface treatment on PA6 polymerization and crystallization

The influence of each silane treatment on the polymerization and crystallization of polyamide 6 was investigated by DSC. The composites were prepared with untreated and treated particles, the neat resin results being provided as a reference.

3.2.1. Influence on PA6 synthesis kinetics

The DSC thermograms associated to the isothermal synthesis of PA6 in glass particles-filled composites are displayed in Figure 6, for pristine (as received) particles and all 5 types of silanes. The DSC thermogram of the neat resin shows two peaks: the first one is related to monomer polymerization, while the second one corresponds to the crystallization of PA6.¹⁹ In the case of the neat resin, the polymerization and crystallization peaks occur around 3 min and 7 min, respectively.

First, in the presence of untreated particles (Figure 6a), the signal is flat, showing that the polymerization reaction does not occur. This demonstrates the incompatibility of the raw glass surface with anionic PA6 synthesis due to the significant amount of -OH groups. Indeed, labile protons of hydroxyl groups on the glass surface deactivate the catalyst, which inhibits the reaction [12].

The DSC thermograms obtained for the silane-grafted particles are presented in Figure 6b, 6c and 6d. In all cases, polymerization and crystallization take place, ensuring that the treatments and developed protocols are compatible with the synthesis of anionic PA6. In the case of hydrophobic particles treated with TMPS, the reaction is significantly slowed down (Figure 6b): the full process lasts 30 min in the presence of glass particles treated with TMPS, instead

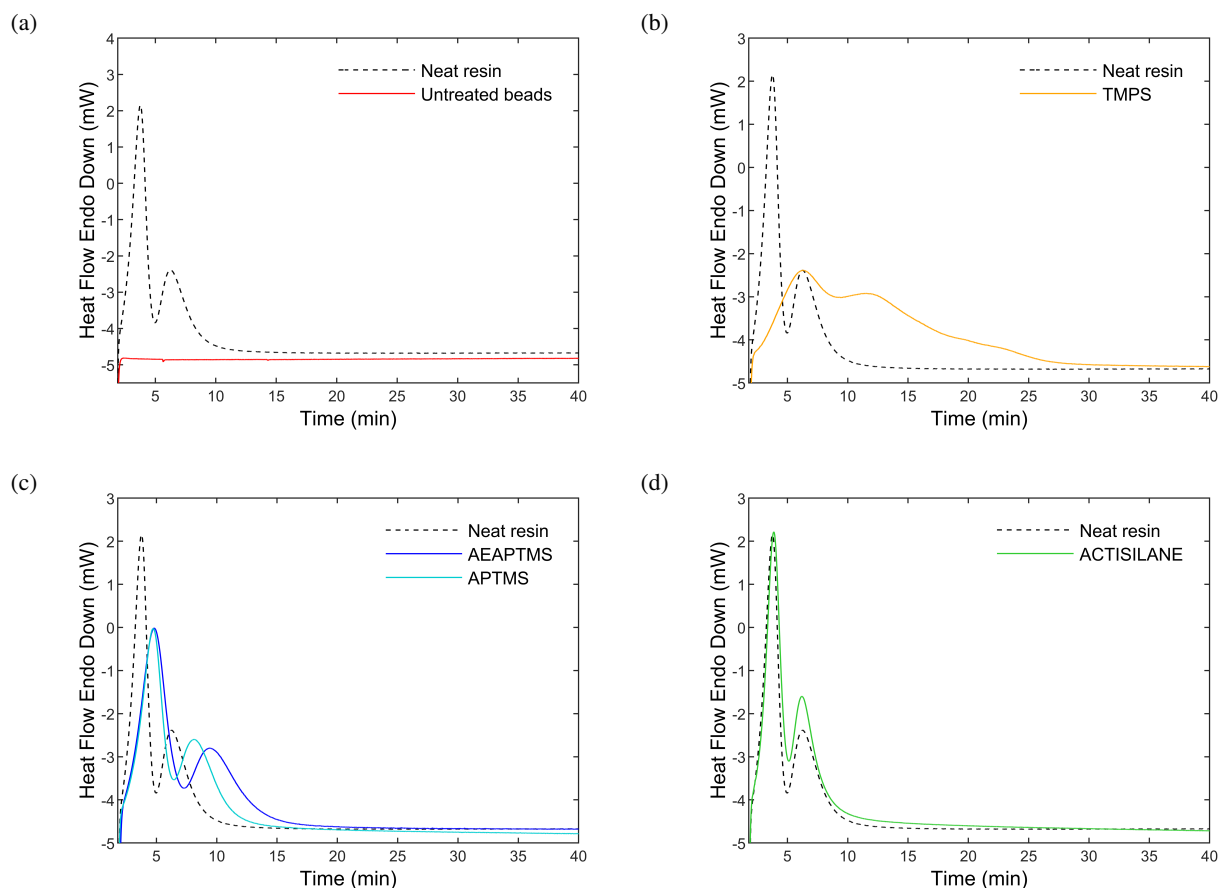


Figure 6: DSC thermograms of isothermal syntheses at 180°C of PA6 and PA6-glass particles composites synthesized with: (a) untreated particles and particles treated with (b) TMPS, (c) APTMS or AEAPTMS, and (d) the ACTISILANE. The neat resin polymerization thermogram is provided as a reference.

of 10 min for the neat resin (300% increase in time). For the particles treated with the aminosilanes (Figure 6c), the reaction is faster than for TMPS, suggesting an increased compatibility between the selected aminosilanes with the AROP reaction. However, the polymerization and crystallization processes remain slower compared to the neat resin, with a 50% increase in synthesis duration. Finally, polymerization and crystallization kinetics for the ACTISILANE treated particles are nearly identical to those of the neat resin, as displayed in Figure 6d. Grafting the activator on the glass particles surface allows to initiate the polymerization directly from the surface of the particles, in addition to the bulk initiation of the AROP. This last result proves that it is indeed possible to synthesize PA6-based glass particles composites, with synthesis features identical to the PA6 resin.

3.2.2. Impact on the conversion degree and crystallization

Next, the degree of conversion and crystallinity of the PA6 matrix were measured. After the isothermal step, the samples were cooled from 180°C to 0°C at $-10^{\circ}\text{C}\cdot\text{min}^{-1}$, and then heated to 270°C at $10^{\circ}\text{C}\cdot\text{min}^{-1}$. Both DSC

thermograms for the cooling and heating steps are shown in Figure 7 for the neat resin, and the composites synthesized either with the untreated or ACTISILANE silanized particles. Note that other samples display thermograms quite similar to those of the ACTISILANE.

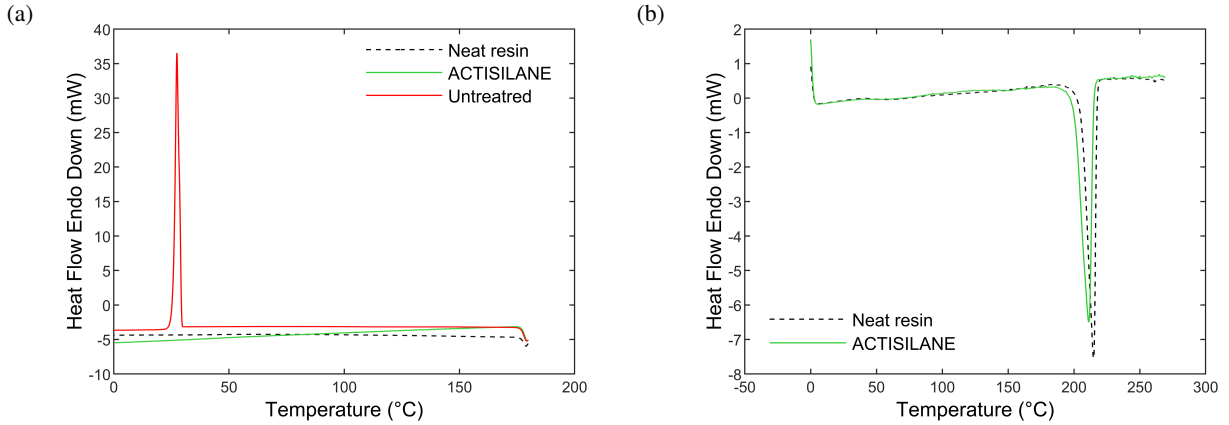


Figure 7: DSC thermograms of PA6 and PA6-glass particle composites synthesized with untreated and ACTISILANE treated particles: (a) cooling step from 180°C to 0°C at $-10^{\circ}\text{C}\cdot\text{min}^{-1}$ and (b) heating step from 0°C to 270°C at $10^{\circ}\text{C}\cdot\text{min}^{-1}$.

During the cooling step, an exothermic peak for the untreated particles indicates the crystallization of unreacted ϵ -caprolactam at 25°C (Figure 7a). This peak is not visible for the neat polymerized resin and ACTISILANE based composite, for which the polymerization reaction is complete. In complement, during the heating step, no exothermic peak that would indicate residual unreacted monomer polymerization was observed for both the neat resin and ACTISILANE treated particles (Figure 7b). This indicates an almost complete consumption of the monomer and, consequently, a very high degree of conversion. However, this information is not sufficient since uncrystallized monomers could remain trapped into the PA6 crystalline lamellas [19].

The melting temperatures determined by DSC are also an indicator of the conversion degree. The results are displayed in Table 6. Khodabakhshi et al. showed that the melting temperature of PA6 depends on the conversion degree [49]. For example, for a melting temperature of 210°C, they measured a conversion degree of 90%, whereas for a temperature of 215°C the conversion reached 96% (a conversion rate of 100% is not achievable) [19, 50, 51]. In our case, the melting temperatures range between 211°C and 215°C, which corresponds to high conversion degrees.

The degree of conversion of ϵ -caprolactam into PA6 can be calculated from the total heat of reaction Q_{tot} obtained from the isotherm step, which is the sum of the polymerization enthalpy ΔH_p^{∞} and the crystallization enthalpy ΔH_m . The latter represents the melting enthalpy measured upon heating during a subsequent step to the isothermal synthesis at 180°C. Hence, the degree of conversion X_p^{∞} is defined according to Equation (3), in which $\Delta H_p^{100\%}$ refers to the total enthalpy of polymerization obtained from Vicard et al. [19] ($\Delta H_p^{100\%} = 123.5 \text{ J}\cdot\text{g}^{-1}$):

Table 6

Melting temperature (T_m), melting enthalpy (ΔH_m), total enthalpy (Q_{tot}), polymerization enthalpy (ΔH_p^∞) and degree of conversion (X_p^∞) of PA6 after the synthesis of PA6/glass particles composites with different types of grafted silanes

| Sample | T_m ($\pm 0.3^\circ$) | ΔH_m ($\pm 0.6 \text{ J.g}^{-1}$) | Q_{tot} ($\pm 1.4 \text{ J.g}^{-1}$) | ΔH_p^∞ ($\pm 0.9 \text{ J.g}^{-1}$) | X_p^∞ ($\pm 0.7\%$) |
|------------|------------------------------|--|---|---|---------------------------------|
| Neat resin | 213.1 | 70.4 | 190.9 | 120.5 | 97.6 |
| TMPS | 215.9 | 72 | 189.9 | 117.9 | 95.5 |
| APTMS | 214.5 | 74.2 | 194 | 119.8 | 97 |
| AEAPTMS | 215.6 | 71 | 189.2 | 118.2 | 95.7 |
| ACTISILANE | 211.2 | 73.5 | 190.6 | 117.1 | 98.5 |

$$X_p^\infty = \frac{Q_{tot} - \Delta H_m}{\Delta H_p^{100\%}} \quad (3)$$

As shown in Table 6, all of the composites prepared with silanized particles lead to a degree of conversion higher than 95%. It is worth noticing that all composites melting enthalpies indicate a very high degree of crystallinity, compared to the bulk crystallization of the neat PA6, as already highlighted in previous studies [19]. This high degree of crystallinity could be attributed to surface induced nucleation.

3.3. Discussion

The grafting protocol that was used to prepare the glass particles surfaces not only ensured an efficient grafting of the selected silanes, but also led to a high degree of conversion of the ϵ -caprolactam monomer ($\approx 95\%$). This demonstrates that a thorough control over the surface hydroxyl density for the entire silanization process prevents activator deactivation and makes it possible to achieve a proper polymerization of the reactive mixture.

The nature of the silane strongly affects the surface density of the grafted silane. Among the silanes studied in this work, TMPS leads to the highest grafting density (Table 4), while AEAPTMS, which contains primary and secondary amine functions, results in the lowest one. In addition to the influence of the silane molecular size, these results also depend on the hydrolysis-condensation kinetics (which depends on silane type), and on the secondary reactions that may occur during silanisation. In particular, horizontal and vertical polymerization catalyzed by the presence of amine groups, and the resulting steric hindrances, may explain this result. Depending on the involved phenomena, one can obtain different grafting densities for different aminosilanes. Indeed, APTMS is more susceptible to form local multilayers of amines by vertical polymerization [32], while AEAPMS has a longer alkyl chain, which favors a more homogeneous aminated surface [26]. Despite the higher grafting density of APTMS (as attested by the TGA results, Table 4), the higher steric hindrance for surface modified by this silane yields to lower fluorescence intensity compared to AEAPTMS (Figures 3 and 4).

Although the significant differences in surface grafting densities could impact the hydrophilic/hydrophobic character of the glass particles, the contact angles are consistent with the nature of the silanes. TMPS renders the surface hydrophobic, while the amine functions in the aminosilanes and ACTISILANE yield more hydrophilic surfaces (Figure 5) and thus improve the interfacial affinity with the hydrophilic monomer.

This specific effect of the silanes functions on the polymerization reaction and crystallization transformation is also highlighted in Figure 6. The hydrophobic character of the TMPS-treated particles substantially slows down polymerization, whereas the reaction time is only increased by about 50% with hydrophilic aminosilanes. Since these silanes are not directly involved in the polymerization reaction, this delay appears to be correlated to the wettability of the glass surface.

As demonstrated in previous works, the presence of NH_2 groups in aminosilanes leads to the formation of hydrogen bonds at the particle-matrix interface between the PA6 carbonyls and the amines of the silane [52]. In addition, the reaction kinetics can be influenced by crystal nucleation at the particle surface during the polymerization process, but also by the species diffusing in the reaction mixture around the glass particles - all features that must be sensitive on the particle surface chemistry. As illustrated in Figure 6c, the DSC thermograms obtained for aminosilanes treated particles show identical polymerization peaks. Even if the type of aminosilane seems to have no effect on the PA6 polymerization, the polymerization kinetics for both aminosilanes is slower than for neat resin. This is most likely a diffusion limited effect of the monomer, oligomers and macromolecules into the material, due to their affinity with the glass surface and to the spatial hindrance caused by the glass particles themselves. This explanation is also consistent with the slower kinetics observed in the presence of TMPS-grafted particles. Due to the decrease of the chemical affinity of the glass surface with the monomers, the spatial hindrance of these particles is increased, which in turn further limits the diffusion process of the reactive species without affecting the final conversion degree. Regarding the crystallization kinetics, one can note, subtly yet clear differences between APTMS and AEAPTMS aminosilanes treatments. This illustrates that the silane type and grafting levels influence the crystallization process, including nucleation effect differences at the glass surface.

In the case of the ACTISILANE grafted particles, the synthesis kinetics is similar to the neat resin. In this case, the glass particles do not induce any particular hindrance to the reactive species diffusion. In contrast with the other tested silanes, the grafted activator allows the glass surface to participate to the reaction and polyamide chains are directly initiated from the surface. The presence of the activator on the glass surface globally increases the concentration of activator in the reactive mixture, consequently increasing the mixture reactivity [23]. This higher reactivity must counterbalance the spatial hindrance of the glass particles, leading to a synthesis time practically identical to that of the neat resin.

The original approach developed in this work consists in initiating the polymerization reaction directly from the surface of the reinforcing particles, allowing to significantly accelerate the synthesis reaction of anionic PA6 based composites in the presence of glass reinforcements. This could also simplify the manufacturing process by eliminating the addition of the activator in the mixture (i.e. eliminating an additional tank containing the mixture of monomer and activator and avoiding the need for a mixing head in the RTM process). Moreover, since the activator is directly grafted at the surface of the glass reinforcement, the treatment of the glass surface with the ACTISILANE can improve the mechanical strength at the interface by creating strong covalent bonds between the glass particles and the matrix. In the end, this could shift the ultimate tensile strength of the composites towards higher values - an aspect that will be analyzed in a forthcoming work.

4. Conclusion

This study demonstrates that the surface chemistry of glass particles significantly impacts the synthesis and crystallization of the anionic PA6 matrix. For silanized particles functionalized with the activator, the polymerization is fast and nearly complete, and crystallization reaches a maximum value comparable to the neat resin thanks to the strong covalent bonds formed between the particles and the matrix at the interface. In contrast, untreated glass particles completely inhibit the polymerization reaction, due to the labile protons of the surface hydroxyls that deactivate the catalyst.

In-between, particles treated with a hydrophobic silane agent considerably slow down the polymerization and crystallization processes of PA6, as compared to the pure resin. In comparison, particles treated with the aminosilanes, which create weak hydrogen bonds at the interface, lead to an acceleration of polymerization and crystallization processes but still display longer times compared to the neat resin or to the particles grafted with the activator-functionalized silane.

This work highlights the importance of controlling the surface chemistry to eventually optimize the polymerization and crystallization processes of anionic polyamide 6-based composites. Initiating the polymerization reaction at the particle surface results in a much shorter synthesis cycle time.

Credit author statement

Achraf Belkhiri : Conceptualization, Methodology, Validation, Investigation, Writing - Original Draft. **Nick Virgilio** : Conceptualization, Methodology, Writing - Review & Editing, Visualization. **Valérie Nassiet** : Visualization, Supervision. **Hélène Weleman** : Writing - Review & Editing, Visualization. **France Chabert** : Conceptualization, Methodology, Writing - Review & Editing, Visualization, Funding acquisition. **Olivier De Almeida** : Conceptualization, Methodology, Writing - Review & Editing, Visualization, Funding acquisition.

Declaration of competing interest

The authors declare that they have no known competing financial interests or personal relationships that could have appeared to influence the work in this paper.

Acknowledgements

- This project was co-funded by the Occitanie region of France, the National Polytechnic Institute of Toulouse (INPT) and IMT Mines Albi through MOVING project
- The authors thank Brüggemann Chemical company, Germany for kindly supplying reactants for the anionic PA6 synthesis.

Supplementary data

Supplementary data can be found in a separate document attached to this article.

References

- [1] A. Bernasconi, D. Rossin, C. Armani, Analysis of the effect of mechanical recycling upon tensile strength of a short glass fibre reinforced polyamide 6,6, *Engineering fracture mechanics* 74 (4) (2007) 627–641.
- [2] T. R. Abdou, D. C. Romano Espinosa, J. A. Soares Tenório, Recovering of carbon fiber present in an industrial polymeric composite waste through pyrolysis method while studying the influence of resin impregnation process: Prepreg, *Rewas 2016: Towards Materials Resource Sustainability* (2016) 311–318.
- [3] F. Henning, H. Ernst, R. Brüssel, Lfts for automotive applications, *Reinforced plastics* 49 (2) (2005) 24–33.
- [4] B. N. Nguyen, S. K. Bapanapalli, J. D. Holbery, M. T. Smith, V. Kunc, B. J. Frame, J. H. Phelps, C. L. Tucker III, Fiber length and orientation in long-fiber injection-molded thermoplastics - Part I: Modeling of microstructure and elastic properties, *Journal of composite materials* 42 (10) (2008) 1003–1029.
- [5] E. M. Silverman, Effect of glass fiber length on the creep and impact resistance of reinforced thermoplastics, *Polymer composites* 8 (1) (1987) 8–15.
- [6] F. Truckenmüller, H.-G. Fritz, Injection molding of long fiber-reinforced thermoplastics: A comparison of extruded and pultruded materials with direct addition of roving strands, *Polymer Engineering & Science* 31 (18) (1991) 1316–1329.
- [7] T. Vu-Khanh, J. Denault, P. Habib, A. Low, The effects of injection molding on the mechanical behavior of long-fiber reinforced PBT/PET blends, *Composites science and technology* 40 (4) (1991) 423–435.

- [8] P. Kiss, W. Stadlbauer, C. Burgstaller, H. Stadler, S. Fehringer, F. Haeuserer, V.-M. Archodoulaki, In-house recycling of carbon-and glass fibre-reinforced thermoplastic composite laminate waste into high-performance sheet materials, *Composites Part A: Applied Science and Manufacturing* 139 (2020) 106110.
- [9] W. Obande, C. M. Ó. Brádaigh, D. Ray, Continuous fibre-reinforced thermoplastic acrylic-matrix composites prepared by liquid resin infusion—a review, *Composites Part B: Engineering* 215 (2021) 108771.
- [10] K. Van Rijswijk, H. Bersee, Reactive processing of textile fiber-reinforced thermoplastic composites - An overview, *Composites Part A: Applied Science and Manufacturing* 38 (3) (2007) 666–681.
- [11] K. Khodabakhshi, M. Gilbert, P. Dickens, R. Hague, S. Fathi, Optimised polymerization conditions for inkjetting of caprolactam to produce polyamide parts, in: 2008 International Solid Freeform Fabrication Symposium, University of Texas at Austin, 2008.
- [12] K. Van Rijswijk, J. Teuwen, H. Bersee, A. Beukers, Textile fiber-reinforced anionic polyamide-6 composites. Part I: The vacuum infusion process, *Composites Part A: Applied Science and Manufacturing* 40 (1) (2009) 1–10.
- [13] S. Bolgov, V. Begishev, A. Y. Malkin, V. Frolov, Role of the functionality of activators during isothermal crystallization accompanying the activated anionic polymerization of ϵ -caprolactam, *Polymer Science USSR* 23 (6) (1981) 1485–1492.
- [14] A. Y. Malkin, V. Frolov, A. Ivanova, Z. Andrianova, The nonisothermal anionic polymerization of caprolactam, *Polymer Science USSR* 21 (3) (1979) 691–700.
- [15] A. Y. Malkin, V. Frolov, A. Ivanova, Z. Andrianova, L. Alekseichenko, The kinetics of anionic polymerization of caprolactam in the presence of carbamylcaprolactams, *Polymer Science USSR* 22 (5) (1980) 1097–1103.
- [16] A. Y. Malkin, S. Ivanova, V. Frolov, A. Ivanova, Z. Andrianova, Kinetics of anionic polymerization of lactams. (solution of non-isothermal kinetic problems by the inverse method), *Polymer* 23 (12) (1982) 1791–1800.
- [17] K. J. Kim, D. S. Hong, A. R. Tripathy, Kinetics of adiabatic anionic copolymerization of ϵ -caprolactam in the presence of various activators, *Journal of applied polymer science* 66 (6) (1997) 1195–1207.
- [18] K. Van Rijswijk, H. Bersee, W. Jager, S. Picken, Optimisation of anionic polyamide-6 for vacuum infusion of thermoplastic composites: choice of activator and initiator, *Composites Part A: Applied Science and Manufacturing* 37 (6) (2006) 949–956.
- [19] C. Vicard, O. De Almeida, A. Cantarel, G. Bernhart, Experimental study of polymerization and crystallization kinetics of polyamide 6 obtained by anionic ring opening polymerization of ϵ -caprolactam, *Polymer* 132 (2017) 88–97.
- [20] K. Van Rijswijk, H. Bersee, A. Beukers, S. Picken, A. Van Geenen, Optimisation of anionic polyamide-6 for vacuum infusion of thermoplastic composites: Influence of polymerisation temperature on matrix properties, *Polymer testing* 25 (3) (2006) 392–404.

- [21] D. Li, Q. Liu, L. Yu, X. Li, Z. Zhang, Correlation between interfacial interactions and mechanical properties of PA-6 doped with surface-capped nano-silica, *Applied Surface Science* 255 (18) (2009) 7871–7877.
- [22] G. Rusu, E. Rusu, Nylon 6/sio₂nanocomposites synthesized by in situ anionic polymerization, *High Performance Polymers* 18 (3) (2006) 355–375.
- [23] K. Van Rijswijk, A. Van Geenen, H. Bersee, Textile fiber-reinforced anionic polyamide-6 composites. Part II: Investigation on interfacial bond formation by short beam shear test, *Composites Part A: Applied Science and Manufacturing* 40 (8) (2009) 1033–1043.
- [24] A. Belkhiri, N. Virgilio, V. Nassiet, H. Weleman, F. Chabert, O. De Almeida, Tailoring the hydroxyl density of glass surface for anionic ring-opening polymerization of polyamide 6 to manufacture thermoplastic composites, *Polymers* 14 (17) (2022) 3663.
- [25] J. L. Thomason, Glass fibre sizing: A review, *Composites Part A: Applied Science and Manufacturing* 127 (August) (2019). doi:10.1016/j.compositesa.2019.105619.
- [26] M. Zhu, M. Z. Lerum, W. Chen, How to prepare reproducible, homogeneous, and hydrolytically stable aminosilane-derived layers on silica, *Langmuir* 28 (1) (2012) 416–423.
- [27] M. Zhang, K. F. Gleich, A. Yohannes, M. J. Block, J. Asrar, Fiber reinforced composites made with coupling-activator treated fibers and activator containing reactive resin, US Patent 10,954,349 (Mar. 23 2021).
- [28] M.-C. Brochier Salon, M. N. Belgacem, Hydrolysis-condensation kinetics of different silane coupling agents, Phosphorus, Sulfur, and Silicon 186 (2) (2011) 240–254.
- [29] A. Legrand, H. Hommel, A. Tuel, A. Vidal, H. Balard, E. Papirer, P. Levitz, M. Czernichowski, R. Erre, H. Van Damme, et al., Hydroxyls of silica powders, *Advances in Colloid and Interface Science* 33 (2-4) (1990) 91–330.
- [30] J. Thomason, D. Dwight, The use of XPS for characterisation of glass fibre coatings, *Composites Part A: Applied Science and Manufacturing* 30 (12) (1999) 1401–1413.
- [31] J. Thomason, The interface region in glass fibre-reinforced epoxy resin composites: 3. Characterization of fibre surface coatings and the interphase, *Composites* 26 (7) (1995) 487–498.
- [32] E. Asenath Smith, W. Chen, How to prevent the loss of surface functionality derived from aminosilanes, *Langmuir* 24 (21) (2008) 12405–12409.
- [33] N. Rathor, S. Panda, Aminosilane densities on nanotextured silicon, *Materials Science and Engineering: C* 29 (8) (2009) 2340–2345.
- [34] J. Zhao, Y. Li, H. Guo, L. Gao, Relative surface density and stability of the amines on the biochip, *Chinese Journal of Analytical Chemistry* 34 (9) (2006) 1235–1238.

- [35] R. G. Acres, A. V. Ellis, J. Alvino, C. E. Lenahan, D. A. Khodakov, G. F. Metha, G. G. Andersson, Molecular structure of 3-aminopropyltriethoxysilane layers formed on silanol-terminated silicon surfaces, *The Journal of Physical Chemistry C* 116 (10) (2012) 6289–6297.
- [36] T. S. Zemanian, G. E. Fryxell, J. Liu, S. Mattigod, J. A. Franz, Z. Nie, Deposition of self-assembled monolayers in mesoporous silica from supercritical fluids, *Langmuir* 17 (26) (2001) 8172–8177.
- [37] A. Labrosse, A. Burneau, Characterization of porosity of ammonia catalysed alkoxysilane silica, *Journal of non-crystalline solids* 221 (2-3) (1997) 107–124.
- [38] A. Perro, Synthèse et valorisation de particules colloïdales de morphologie et de fonctionnalité de surface contrôlées, Ph.D. thesis, Université Sciences et Technologies-Bordeaux I (2006).
- [39] M. Szekeres, J. Tóth, I. Dékány, Specific surface area of stoeber silica determined by various experimental methods, *Langmuir* 18 (7) (2002) 2678–2685.
- [40] M. Szekeres, I. Dékány, A. De Keizer, Adsorption of dodecyl pyridinium chloride on monodisperse porous silica, *Colloids and Surfaces A: Physicochemical and Engineering Aspects* 141 (3) (1998) 327–336.
- [41] J. Wells, L. Koopal, A. d. de Keizer, Monodisperse, nonporous, spherical silica particles, *Colloids and Surfaces A: Physicochemical and Engineering Aspects* 166 (1-3) (2000) 171–176.
- [42] A. De Keizer, E. Van der Ent, L. Koopal, Surface and volume charge densities of monodisperse porous silicas, *Colloids and Surfaces A: Physicochemical and Engineering Aspects* 142 (2-3) (1998) 303–313.
- [43] R. De Palma, S. Peeters, M. J. Van Bael, H. Van den Rul, K. Bonroy, W. Laureyn, J. Mullens, G. Borghs, G. Maes, Silane ligand exchange to make hydrophobic superparamagnetic nanoparticles water-dispersible, *Chemistry of Materials* 19 (7) (2007) 1821–1831.
- [44] X.-Y. Wang, D. Mertz, C. Blanco-Andujar, A. Bora, M. Ménard, F. Meyer, C. Giraudeau, S. Bégin-Colin, Optimizing the silanization of thermally-decomposed iron oxide nanoparticles for efficient aqueous phase transfer and MRI applications, *RSC advances* 6 (96) (2016) 93784–93793.
- [45] J. G. Matisons, Silanes and siloxanes as coupling agents to glass: a perspective, *Silicone Surface Science* (2012) 281–298.
- [46] J. González-Benito, J. Baselga, A. Aznar, Microstructural and wettability study of surface pretreated glass fibres, *Journal of Materials Processing Technology* 92 (1999) 129–134.
- [47] K. Sever, Y. Seki, I. H. Tavman, G. Erkan, V. Cecen, The structure of γ -glycidoxypropyltrimethoxysilane on glass fiber surfaces: Characterization by ftir, sem, and contact angle measurements, *Polymer composites* 30 (5) (2009) 550–558.
- [48] W. Xu, J. Riikonen, T. Nissinen, M. Suvanto, K. Rilla, B. Li, Q. Wang, F. Deng, V.-P. Lehto, Amine surface modifications and fluorescent labeling of thermally stabilized mesoporous silicon nanoparticles, *The Journal of*

Physical Chemistry C 116 (42) (2012) 22307–22314.

- [49] K. Khodabakhshi, M. Gilbert, S. Fathi, P. Dickens, Anionic polymerisation of caprolactam at the small-scale via DSC investigations, *Journal of Thermal Analysis and Calorimetry* 115 (1) (2014) 383–391.
- [50] O. Wichterle, J. šebenda, J. Králíček, The anionic polymerization of caprolactam, in: *Fortschritte Der Hochpolymeren-Forschung*, Springer Berlin Heidelberg, Berlin, Heidelberg, 1961, pp. 578–595.
- [51] B. Wunderlich, *Macromolecular physics*, vol. 2, crystal nucleation, Growth, Annealing 3 (1976).
- [52] Y. Li, J. Yu, Z.-X. Guo, The influence of silane treatment on nylon 6/nano-sio₂ in situ polymerization, *Journal of Applied Polymer Science* 84 (4) (2002) 827–834.